

# Probing the shape of hot $^{194}\text{Hg}$ at high spins with the giant dipole resonance decay in selected cascades

F. Camera, A. Bracco, S. Leoni, B. Million, M. Mattiuzzi, and M. Pignanelli

*Dipartimento di Fisica, Università di Milano, and INFN sez. Milano, via Celoria 16, I-20133 Milano, Italy*

A. Maj and M. Kmiecik

*The Henryk Niewodniczański Institute of Nuclear Physics, 31-342 Krakow, Poland*

R. Bark, J. Bearden, and J. J. Gaardhøje

*The Niels Bohr Institute, Copenhagen, Denmark*

W. E. Ormand

*Department of Physics and Astronomy, Louisiana State University, Baton Rouge, Louisiana 70803-4001*

T. Lönnroth and R. Österbacka

*Department of Physics, Åbo Akademi, FIN-20500 Turku, Finland*

(Received 5 October 1998; published 16 June 1999)

High-energy  $\gamma$  rays emitted by the decay of the hot compound nucleus  $^{194}\text{Hg}$ , formed in the reaction  $^{30}\text{Si}(142\text{ MeV}) + ^{164}\text{Dy}$ , have been measured in coincidence with different residual nuclei. The measured spectra and the relative residual-nucleus cross sections were simultaneously analyzed with the statistical model. Calculations assuming contributions from a GDR in superdeformed states were also made. No clear evidence was found that superdeformed shapes seen at  $T=0$  survive at average nuclear temperature  $\langle T \rangle \approx 1.3\text{ MeV}$ . Instead, an average nuclear deformation corresponding to  $\langle \beta \rangle = 0.3$  constant with spin has been deduced for  $20 < I < 38\ \hbar$  by comparing the measured width to that predicted by the model of thermal shape fluctuations. [S0556-2813(99)04107-2]

PACS number(s): 21.60.Ka, 21.10.Re, 23.20.Lv, 24.30.Cz

## I. INTRODUCTION

One of the central questions in the field of nuclear structure is that concerning the nuclear motion as a function of temperature. This question is being addressed by studying the properties of the giant-dipole resonance (GDR) at finite excitation energy. Experimentally several efforts have been made to improve the selectivity of these studies by measuring the  $\gamma$  decay of the GDR associated to specific region of the phase space available for the decay of highly excited nuclei. The selectivity concerns angular momentum (see, e.g., Refs. [1–3]), excitation energy (see, e.g., Ref. [4]), and the final residual nucleus (see, e.g., Refs. [5,6]). In general, the comparison of the experimental findings with model predictions yields information on the average nuclear shape at finite temperature and angular momentum, on the role of thermal shape fluctuations and on the damping mechanisms of this collective mode at finite temperature [7]. More recently, the width of the GDR was studied as a function of temperature and angular momentum keeping one of the two quantities fixed [2,3]. The width of the GDR was found to reflect the average nuclear deformation [2,8]. In particular, the studies of  $^{106}\text{Sn}$  and  $^{176}\text{W}$  at  $T < 2\text{ MeV}$  have shown that the influence of the rotational angular momentum on the width of the GDR is strongly dependent on the nuclear moment of inertia. In fact, for nuclei as heavy as  $^{176}\text{W}$  angular momentum effects are unimportant because the average nuclear deformation does not change significantly with increasing  $I$ .

On the basis of the previous discussion it becomes interesting to study a nucleus such as  $^{194}\text{Hg}$ . In fact, since this nucleus is heavier than  $^{176}\text{W}$ , it allows us to check the expectation that at moderate temperature ( $T = 1.0\text{--}1.5\text{ MeV}$ ) the average nuclear deformation of nuclei in the mass region  $A = 190\text{--}200$ , due to the large moment of inertia, should be relatively small and should not change with increasing angular momentum. This behavior is in contrast with that at  $T = 0$  where for Hg and Pb isotopes a number of superdeformed bands were found at high spins. A detailed study of the  $\gamma$  decay of the GDR for a heavy nucleus such as  $^{194}\text{Hg}$  is therefore interesting to test whether or not the strong effects induced at  $T = 0$  by angular momentum can persist at moderate temperature ( $T < 1.5\text{ MeV}$ ) or if they largely influence the value of the nuclear average deformation. Because of the present interest on the problem of superdeformation it is important to establish, in the best possible way, the properties of hot compound nuclei whose decay leads to the population of superdeformed configurations.

Concerning this mass region two works were made at the beginning of the 1990's. One is mainly focused on the properties of the pre-fission and post-fission GDR emission [9], in contrast with the present measurement of  $^{194}\text{Hg}$  for which the fusion-evaporation channel is strongly populated and cleanly selected. The second, concerning the nucleus  $^{190}\text{Hg}$  at lower excitation energy [10], was rather limited in statistics so that it was not possible to obtain (and consequently to reproduce with the statistical model) the cross section of the different residual nuclei as a function of  $\gamma$ -ray energy in the

region of interest for the GDR. This point, which is instead discussed in the present paper, is important since it provides a more complete test for the statistical  $\gamma$  decay of compound nuclei, which is the basic assumption of all GDR studies at finite temperature.

A recent work reported in Ref. [11], relative to the decay of the compound nucleus  $^{148}\text{Gd}$ , showed that the statistical model could not reproduce  $\gamma$  yields and the total production yields for the different evaporation residues unless the excitation energy of the compound is lowered by  $\approx 6$  MeV. Consequently more detailed studies, also in other mass regions, in which a simultaneous analysis is made for the high-energy  $\gamma$ -ray spectra and for the cross section of the different residual nuclei as a function of  $\gamma$ -ray energy, provide not only a consistency check for the deduced value of the GDR parameters but also a more stringent test for the present knowledge of the fusion-evaporation process. The latter is an important point, since in a number of cases the emission of high-energy  $\gamma$  rays has been employed to study the mechanisms leading to the fusion and fission processes (see, e.g., Refs. [12–14]). In particular, the problem of the entrance channel effects has been extensively studied and in one of the latest work [15] the measurement of the  $\gamma$  decay of the GDR in  $^{156}\text{Er}$  in coincidence with the low-energy  $\gamma$  transitions of the most populated residual nucleus has been used. However, in that case a simultaneous analysis of the high-energy  $\gamma$ -ray spectra and of the cross section of the different residual nuclei as a function of  $\gamma$ -ray energy was not made. In addition, the statistical model analysis was made without using the Monte Carlo approach which is instead required in the case of channel selection.

## II. EXPERIMENT

The experiment was performed at the Tandem Accelerator Laboratory of the Niels Bohr Institute (Risø, Denmark). The reaction was  $^{30}\text{Si} + ^{164}\text{Dy}$  at bombarding energy 142 MeV. The target thickness was  $0.75 \text{ mg/cm}^2$  (with a purity of 98.4% in the isotope  $^{164}\text{Dy}$ ). The corresponding excitation energy for the compound nucleus  $^{194}\text{Hg}$  is 60 MeV and the maximum angular momentum  $41 \hbar$ . The experimental apparatus used was a combination of the Nordball detector array (17 Compton-suppressed Ge detector with a 30 element multiplicity filter) and the HECTOR detector array. The latter consists of eight large volume  $\text{BaF}_2$  detectors for the measurement of high-energy  $\gamma$  rays [16]. Neutron and  $\gamma$  separation was obtained by measuring the time of flight from the target. Gain shifts were monitored to better than 0.2% using an LED system optically coupled to the large  $\text{BaF}_2$  crystals by optic fibers, and corrected off line as necessary. The energy calibration of the high-energy detectors was done using the 15.1 MeV  $\gamma$  rays from  $\text{D}(^{11}\text{B}, n\gamma)^{12}\text{C}^*$  reaction as a high-energy point and utilizing the zero suppression mode of the ADC. The detection efficiency for high-energy  $\gamma$  rays was  $\approx 1\%$  at 15 MeV, similar to that for the detection of low-energy  $\gamma$  rays. The collected events ( $2.5 \cdot 10^7$ ) consisted of the coincidence between a high-energy  $\gamma$  ray ( $E_\gamma > 3$  MeV), and at least one low-energy  $\gamma$  ray detected in the Ge detector array together with two or more low-energy  $\gamma$

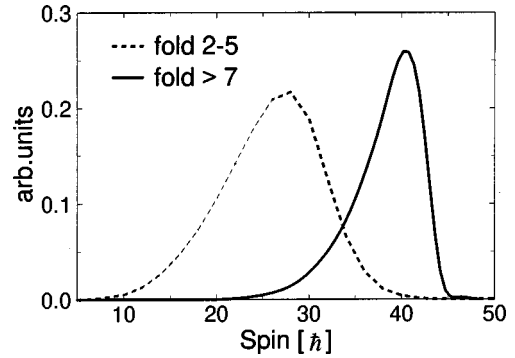


FIG. 1. The lines show the expected spin distribution corresponding to the fold intervals  $2 \leq F_\gamma \leq 5$  (dashed line) and  $F_\gamma > 7$  (full line).

rays detected in the multiplicity filter.

The multiplicity filter covered a solid angle of  $\approx 2\pi$ . In Fig. 1 we show the spin distributions associated with the two different fold intervals selected for the study of the spin dependence of the width of the GDR discussed below. The conversion between the measured coincidence fold  $F_\gamma$  (the number of measured coincident  $\gamma$  rays of low energy in one event) with the multiplicity  $M_\gamma$  (the number of  $\gamma$  rays emitted in the reaction) was established with the procedure described in Ref. [16] using for the efficiency of the filter the value  $\approx 35\%$  (as measured with radioactive sources) and including the effect of the coincidence with at least one  $\gamma$  ray in the germanium detectors and of the window selection in sum energy. The conversion from multiplicity to angular momentum was done assuming  $J = 2M + 2$ , taking into account that neutron emission is the main evaporation channel. The two curves in Fig. 1 are well separated and correspond to  $2 \leq F_\gamma \leq 5$  (dashed line) and  $F_\gamma > 7$  (full drawn line) with average value 24 and 36  $\hbar$ , respectively.

Figure 2 shows low-energy  $\gamma$ -ray Ge spectra for different conditions on the energy measured in  $\text{BaF}_2$  detectors. One (lower spectrum in top panel) is in coincidence with high-energy  $\gamma$  rays with  $E_\gamma > 3$  MeV and the other (upper spectrum in top panel) with  $E_\gamma > 10$  MeV. In these spectra one can readily see that the relative intensity of the low-spin transitions of the populated residual nuclei  $^{190}\text{Hg}$  ( $4n$  channel),  $^{189}\text{Hg}$  ( $5n$  channel), and  $^{191}\text{Hg}$  ( $3n$  channel) depends on the energy of the gating transition. In particular, when the condition  $E_\gamma > 3$  MeV is required the most populated channels are the  $4n$  and  $5n$  while the population of the  $3n$  channel is very small. Instead, a gate with  $E_\gamma > 10$  MeV enhances the  $3n$  channel, as seen in Fig. 2, since the high-energy  $\gamma$  rays replace a neutron in the decay sequence. Consequently, the spectrum associated with the  $3n$  channel (or in general the channel that is the least populated when no conditions on high-energy  $\gamma$  rays are required) is the most interesting for the GDR study in hot nuclei because in this spectrum the contribution of high-energy  $\gamma$  rays is enhanced. Indeed, the selection of this decay channel allows us to reject a large fraction of the cascades containing only  $\gamma$  rays with  $E_\gamma < 7-8$  MeV that are mainly emitted at the end of the decay and that constitute a background for the study of the GDR in the hot compound. This can be seen in Figs. 3 and 4

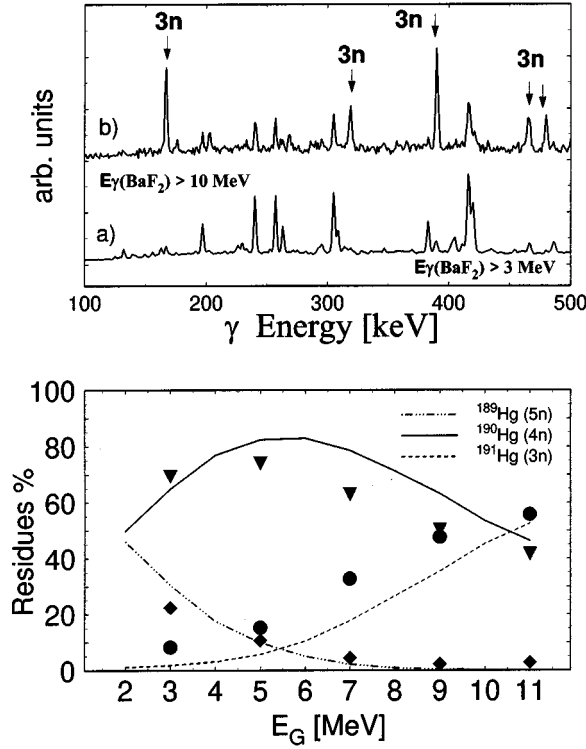


FIG. 2. Top part: Two  $\gamma$ -ray spectra measured for the reaction  $^{30}\text{Si}$  (142 MeV) +  $^{164}\text{Dy}$  with Ge detectors. Spectrum (a) is in coincidence with high-energy  $\gamma$  rays with energy  $E_{\gamma} > 3$  MeV and (b) is in coincidence with high-energy  $\gamma$  rays with energy  $E_{\gamma} > 10$  MeV. Bottom part: Fractions of residue cross sections, deduced from the intensity of the low-energy  $\gamma$  rays in the Ge spectra in coincidence with a  $\gamma$  ray with an energy  $E_G$  or higher. The filled diamonds correspond to  $^{189}\text{Hg}$ , the filled triangles to  $^{190}\text{Hg}$ , and the filled circles to  $^{191}\text{Hg}$ . The lines are the results of statistical model calculations of Monte Carlo type.

where the high-energy  $\gamma$ -ray spectrum in coincidence with the  $3n$  channel is compared to the total spectrum (namely the spectrum in coincidence with the low-spin transitions of all open channels). In these figures the spectrum associated to the  $3n$  channel has been scaled to the same number of counts as the total spectrum in the GDR region ( $E_{\gamma} = 13$ – $15$  MeV) to emphasize the difference in spectral shape and slope of the two spectra in the region  $E_{\gamma} < 8$  MeV.

### III. DATA ANALYSIS AND RESULTS

All measured spectra were analyzed within the framework of the statistical model decay of the compound  $^{194}\text{Hg}$  nucleus. Because of the channel selection a Monte Carlo approach is necessary [10]. This approach has reproduced very well the multiplicity of high-energy  $\gamma$  rays in the  $A = 90$  mass region [17]. A first but critical and stringent test for this type of calculations is the comparison of the calculated distribution of residual nuclei as a function of the energy range ( $E_{\gamma} > E_G$ ) of the coincident high-energy  $\gamma$  ray. The measured values, obtained evaluating the intensity of the

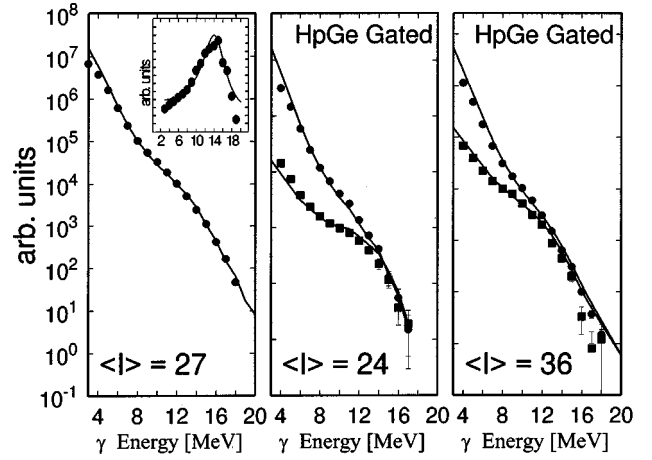


FIG. 3. Measured spectra in comparison with statistical model calculations (full lines). The total spectrum (that is gated by all lines of the different residues) is shown with filled circles while the  $3n$  spectrum with filled squares. The left panel shows the data with no condition from the multiplicity filter and the best fitting statistical model calculation with one Lorentzian strength function corresponding to  $E_{\text{GDR}} = 14.0$  MeV and  $\Gamma_{\text{GDR}} = 6.5$  MeV. In the inset the quantity  $F(E_{\gamma})Y_{\gamma}^{\text{exp}}(E_{\gamma})/Y_{\gamma}^{\text{cal}}(E_{\gamma})$  is plotted.  $Y_{\gamma}^{\text{exp}}(E_{\gamma})$  is the experimental spectrum and  $Y_{\gamma}^{\text{cal}}(E_{\gamma})$  the best fit calculated spectrum, corresponding to the single Lorentzian function  $F(E_{\gamma})$ . In the central and right panels the spectra associated with two different spin windows  $\langle I \rangle = 24 \hbar$  and  $\langle I \rangle = 36 \hbar$  are shown. The calculations use a single Lorentzian function ( $E_{\text{GDR}} = 14$  MeV and  $\Gamma_{\text{GDR}} = 6.5$  MeV for  $\langle I \rangle = 24 \hbar$  and  $E_{\text{GDR}} = 14$  MeV and  $\Gamma_{\text{GDR}} = 5.5$  MeV for  $\langle I \rangle = 36 \hbar$ ).

transitions for the first excited states in  $^{189}\text{Hg}$ ,  $^{190}\text{Hg}$ , and  $^{191}\text{Hg}$  residual nuclei, are shown in the bottom part of Fig. 2 together with the calculations. All channels are rather well predicted in the two different spin windows and in the total case. The GDR width was varied to reproduce, simulta-

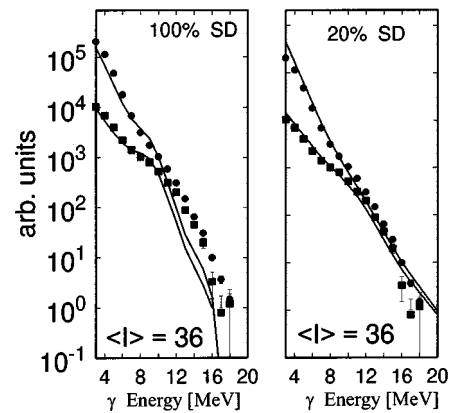


FIG. 4. Measured spectra in comparison with statistical model calculations (full lines). The total spectrum (which is gated by all lines of the different residues) is shown with filled circles while the  $3n$  spectrum with filled squares. The left panel shows calculations at  $\langle I \rangle = 36 \hbar$  using a two Lorentzian function for the superdeformed nucleus ( $E_{\text{GDR1}} = 9.8$  MeV,  $\Gamma_{\text{GDR1}} = 3$  MeV and 33% of the EWSR,  $E_{\text{GDR2}} = 15.8$  MeV,  $\Gamma_{\text{GDR2}} = 7$  MeV, and 66% of the EWSR) in 100% of the cascades while in the right panel in 20%.

neously, the total spectrum and those associated to the different final channels in two spin windows. A level density parameter of  $a=A/8$  MeV and 100% of the EWSR strength was used.

A single Lorentzian analysis was carried out for the spectra corresponding to fold equal or larger than 2 (total measured fold of the multiplicity filter) and for the fold intervals 2–5 and  $>7$ . In the left panel of Fig. 3 the spectrum associated with the total measured fold distribution is shown in comparison with the statistical model calculation corresponding to  $E_{\text{GDR}}=14$  MeV and  $\Gamma_{\text{GDR}}=6.5$  MeV. The GDR centroid value is similar to that of the ground state (13.7 MeV) and to that reported in Ref. [10]. In the center and right panels we show data and calculations for the total spectrum (gated by all lines) and for the  $3n$  channel. They correspond to  $E_{\text{GDR}}=14$  MeV and  $\Gamma_{\text{GDR}}=6.5$  MeV for the  $\langle I \rangle=24 \hbar$  case and to  $E_{\text{GDR}}=14$  MeV and  $\Gamma_{\text{GDR}}=5.5$  MeV for the  $\langle I \rangle=36 \hbar$  case.

The  $3n$  channel spectrum, being rather flat, should display an enhanced sensitivity to the details of the low-energy tail of the GDR with respect to the total spectrum. Therefore, we have performed also statistical model calculations assuming a contribution of the GDR in superdeformed states for  $\langle I \rangle=36 \hbar$  data. The superdeformed strength function was taken as a two Lorentzian function, one with  $E_{\text{GDR}1}=9.8$  MeV,  $\Gamma_{\text{GDR}1}=3$  MeV, and 33% of the EWSR strength and the other with  $E_{\text{GDR}2}=15.8$  MeV,  $\Gamma_{\text{GDR}2}=7$  MeV, and 66% of the EWSR strength. These calculations are shown in Fig. 4. In the left panel of Fig. 4 we show the calculation assuming that the nucleus is superdeformed in all cascades while in the right panel only in 20% of the decay cascades. In this connection it is important to remember that the intensity for the population of superdeformed configurations around the yrast line has been found to be much larger than that of the population of the superdeformed yrast transitions [18]. The normal deformed case is preferred [being the value of the  $\chi^2$  in the interval (7–16 MeV)  $\approx 30\%$  smaller in the case of a single Lorentzian] although one cannot exclude possible contributions of the order of  $\approx 10\%$  from the decay of GDR in a superdeformed configuration. However, at this level it is difficult to infer the presence of such a superdeformed contribution, particularly because the uncertainty with which we reproduce the residual distribution is larger than 10%, and consequently altogether the single Lorentzian analysis is more reliable.

Theoretical calculations of the GDR strength function were carried out under the assumption of an adiabatic coupling between the GDR and the nuclear quadrupole deformation [19,20] while projecting the third component of the angular momentum. The precise details in which the model was implemented are given in Ref. [20], and are only briefly described here. The underlying assumptions in the model are that all deformations and orientations are thermally excited in the compound nucleus and that the time scale associated with thermally induced fluctuations of the deformation and orientation of the system is slow enough so as to not directly affect the GDR strength function. The base model for the GDR then consists of three fundamental modes corresponding to vibrations along each of the intrinsic axes with a cen-

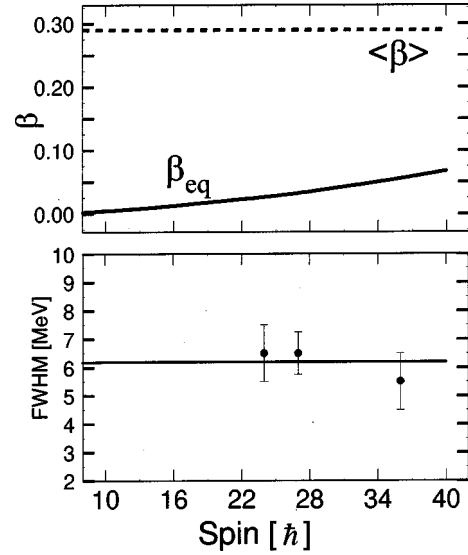


FIG. 5. The deduced GDR width at  $\langle T \rangle=1.3$  MeV as a function of angular momentum in comparison with the thermal shape fluctuation predictions described in the text (full line). In the top part of the figure the equilibrium deformation (that minimizes the Free energy) and the average deformation of  $^{194}\text{Hg}$  are shown.

troid energy  $E_k=R_0/R_k$ , where the intrinsic radius  $R_k$  is given by the Hill-Wheeler formula [20], and an intrinsic damping width of  $\Gamma_k=\Gamma_0^\perp(E_k/E_{\text{GDR}})^\delta$ , where, for  $^{194}\text{Hg}$ , the values  $E_{\text{GDR}}=13.5$  MeV,  $\Gamma_0^\perp=4.0$  MeV, and  $\delta=1.9$  were used. The total strength function is calculated as a superposition of the strength functions obtained at each deformation and orientation weighted by the Boltzmann factor  $\exp(-F/T)$ .  $F$  denotes the free energy, which is a function of the quadrupole shape variables  $\beta$  and  $\gamma$ , the temperature  $T$ , the angular momentum  $I$ , and the Euler angles  $\theta, \phi, \psi$  describing the orientation of the nucleus. The nuclear free energies were computed within the framework of the Nilsson-Strutinsky [21–23] procedure. The averaging has been done by integrating over the five degrees of freedom using the volume element  $\beta^4 \sin 3\gamma d\beta d\gamma \sin \theta d\theta d\phi d\psi$  using Monte Carlo methods.

The thermal averaging predicts a broadening of the GDR strength function that is in overall good agreement with experimental findings, as can be seen in Fig. 5. This broadening reflects the increase of the calculated average nuclear deformation at finite temperature, with respect to the nearly spherical shape at  $T=0$  MeV. In the top part of Fig. 5, we show the average value of  $\beta$ , which, in this case, is approximately 0.3 and essentially independent of  $I$ . As  $I$  increases, the nucleus tends to undergo oblate flattening due to centrifugal effects. The magnitude of the minimum of the Free energy, occurring at the equilibrium deformation (see Fig. 5) is determined by the interplay between the surface and the rotational energy, and is sensitive to the moment of inertia of the system. Because of the dependence in the free energy on the inverse of the moment of inertia, for heavy nuclei, such as  $^{194}\text{Hg}$ , the influence of oblate flattening on the GDR strength function should be reduced since the mean value of the deformation does not change appreciably as a function of

angular momentum. As a consequence, the principal mechanism behind the broadening of the GDR strength function is the increased sampling of quadrupole deformations with temperature and not the increased angular momentum. Indeed, the width of the GDR deduced from calculations that included only thermal shape effects reproduces the data quite well.

#### IV. CONCLUSIONS

In summary, conclusions on three points related to the study of the  $\gamma$  decay of the GDR in hot rotating nuclei are obtained. The first is that the measured GDR width reflects the average shape of the nucleus which, in agreement with the model of thermal shape fluctuations, does not change with increasing angular momentum. The present result, when compared with the work on light and medium mass nuclei [2,24] shows that angular momentum effects depend on the nuclear moment of inertia. The second is that this experiment has provided a more complete test of the statistical model decay of high-energy  $\gamma$  rays which has been shown to reproduce simultaneously the spectra associated with different

channels and residual distribution yields. The last point is that there is no convincing evidence of superdeformed shapes at high spins and at this temperature  $\langle T \rangle = 1.3$  MeV, neither in the total spectrum nor in the  $3n$  spectrum that has a particularly enhanced sensitivity to the low-energy tail of the hot GDR strength function. The fact that the possible contribution of a superdeformed GDR in the high-energy spectrum associated to a particular residue is small suggests the need for a better cascade selection, as for instance by choosing cascades leading to different configurations (SD and non-SD) of the same residual nucleus [25]. Consequently, the problem of the GDR in superdeformed nuclei remains an interesting topic to be addressed with more powerful experimental arrays such as, for example, EUROBALL and GAMMASPHERE.

#### ACKNOWLEDGMENTS

W.E.O. acknowledges support from NSF Cooperative agreement No. EPS 9550481, NSF Grant No. 9603006, and DOE Contract No. DE-FG02-96ER40985. A.M. acknowledges support from Polish KBN Grant No. 2 P03B 001 16.

- 
- [1] Z.M. Drebi *et al.*, Phys. Rev. C **52**, 578 (1995).
  - [2] M. Mattiuzzi *et al.*, Nucl. Phys. **A612**, 262 (1997); A. Bracco *et al.*, Phys. Rev. Lett. **74**, 3748 (1995).
  - [3] E. Ramakrishnan *et al.*, Phys. Rev. Lett. **76**, 2025 (1996); E. Ramakrishnan *et al.*, Phys. Lett. B **383**, 252 (1996).
  - [4] A. Maj *et al.*, Phys. Lett. B **291**, 385 (1992).
  - [5] A. Stolk *et al.*, Nucl. Phys. **A205**, 241 (1989).
  - [6] R.F. Noorman *et al.*, Phys. Lett. B **292**, 257 (1992).
  - [7] P.F. Bortignon, A. Bracco, and R.A. Broglia, in *Giant Resonances: Nuclear Structure at Finite Temperature* (Gordon Breach, New York, 1998).
  - [8] W.E. Ormand *et al.*, Nucl. Phys. **A614**, 217 (1997).
  - [9] R. Butsch *et al.*, Phys. Rev. C **41**, 1530 (1990).
  - [10] A. Atac *et al.*, Phys. Lett. B **252**, 545 (1990).
  - [11] L.H. Zhu *et al.*, Nucl. Phys. **A635**, 325 (1998).
  - [12] P. Paul and M. Thoennessen, Annu. Rev. Nucl. Part. Sci. **44**, 65 (1994).
  - [13] M. Thoennessen *et al.*, Phys. Rev. Lett. **70**, 4055 (1993).
  - [14] S. Flibotte *et al.*, Phys. Rev. C **53**, R533 (1996).
  - [15] M. Cinausero *et al.*, Nucl. Phys. **A599**, 111C (1996); G. Viesti *et al.*, *ibid.* **A604**, 81 (1996).
  - [16] A. Maj *et al.*, Nucl. Phys. **A571**, 185 (1994).
  - [17] M.G. Herman *et al.*, Phys. Lett. B **203**, 29 (1988).
  - [18] S. Leoni *et al.*, Phys. Rev. Lett. **76**, 3281 (1996).
  - [19] Y. Alhassid and N. Whelan, Nucl. Phys. **A565**, 427 (1993).
  - [20] W.E. Ormand *et al.*, Phys. Rev. Lett. **77**, 607 (1996); Nucl. Phys. **A614**, 217 (1997); **A618**, 20 (1997).
  - [21] V.M. Strutinsky, Yad. Fiz. **3**, 614 (1966) [Sov. J. Nucl. Phys. **3**, 449 (1966)]; Ark. Fys. **36**, 629 (1966); Nucl. Phys. **A95**, 420 (1967); **A122**, 1 (1968).
  - [22] S.G. Nilsson *et al.*, Nucl. Phys. **A131**, 1 (1969).
  - [23] C. Guet *et al.*, Phys. Lett. B **205**, 427 (1988).
  - [24] D. Kusnezov, Y. Alhassid, and K.A. Snover, Phys. Rev. Lett. **81**, 542 (1998), and references therein.
  - [25] F. Camera *et al.*, Eur. Phys. J. A **2**, 1 (1998).